Mantle Petrology: Field Observations and High Pressure Experimentation: A Tribute to Francis R. (Joe) Boyd
© The Geochemical Society, Special Publication No. 6, 1999
Editors: Yingwei Fei, Constance M. Bertka, and Bjorn O. Mysen

Conditions of magma generation for Archean komatiites from the Barberton Mountainland, South Africa

TIMOTHY L. GROVE,[1] STEPHEN W. PARMAN[1] and JESSE C. DANN,[2]

[1]Department of Earth and Planetary Sciences, Massachusetts Institute of Technology, Cambridge, MA 02139 USA
[2]Department of Geological Sciences, University of Cape Town, Rondebosch 7700 South Africa

Abstract—This paper evaluates the significance of major element compositional variations and mineralogical evidence in the olivine spinifex komatiites of the 3.49 Ga Komati Formation of the Barberton Mountainland, South Africa. Constraints derived from bulk rock and mineral chemical composition are used to infer the conditions of komatiite crystallization near the Earth's surface and melt production in the mantle source. The emphasis is on the 3.49 Ga komatiites of the Barberton Mountainland, South Africa, but we compare these rocks with other younger (2.6–2.7 Ga) komatiites from Munro and Boston Townships, Canada. Because all Archean komatiites are metamorphosed, the influence of metamorphic processes on the composition of the igneous protolith must be critically evaluated. We document the effects of open system metamorphic serpentinization. We also show how we identify the composition that is closest to the igneous protolith. We also apply the results of phase equilibrium experiments to interpret the compositional information preserved in igneous minerals in komatiites. New experimental data on a primitive Barberton komatiite composition containing 6 wt. % H_2O is used to infer the temperature - depth regime of melt generation. The liquidus phase relations were determined in AuPd alloy capsules from 2 to 2.5 GPa in a piston cylinder device. The komatiite composition is multiply saturated on its liquidus with olivine and orthopyroxene at 2.2 GPa and 1430°C. These average melting conditions provide a basis for evaluating mantle melting models for hydrous komatiite magmas. The favored regime for melt generation is an Archean subduction zone. In this model H_2O is supplied by dewatering of the slab. The H_2O rises into overlying hotter mantle and melting begins at near H_2O-saturated conditions. The melt separates and ascends into the hotter, shallower portion of the wedge. The melt reacts with this mantle, producing additional melt and diluting its H_2O content. Melting progresses until the magma reaches the hottest part of the wedge and the final melt resembles a batch melt. The unique compositional characteristics of the Barberton komatiites result from higher H_2O or higher temperature, or a combination of both, in the Archean arc environment. Based on the depth range of melting, the favored source mantle is one that was depleted by a prior melt extraction process.

INTRODUCTION

KOMATIITES are high MgO (18–33 wt. %) igneous rocks that are found predominantly in Archean and early Proterozoic greenstone belts ARNDT and NISBET (1982). Komatiites are one candidate for the melt that was removed from Archean mantle to produce the depleted harzburgite residues that constitute stable buoyant tectosphere BOYD (1989). These igneous rocks are also important, because the high anhydrous liquidus temperature inferred for some komatiites (1670°C, GREEN *et al.*, 1975) provide the only direct evidence for high Archean mantle temperatures. These high-MgO melts of the mantle are most abundant in Archean and early Proterozoic greenstone belts and rare in the Phanerozoic record. Thus, they represent a set of magma generation conditions in the early Earth that may no longer be operative, or that may operate only in rare circumstances. The assumed high liquidus temperatures of komatiites were questioned by ALLEGRE (1982), who proposed that the presence of dissolved magmatic H_2O might lower the temperature required to produce komatiites. Petrologic evidence provides support for Allegre's hypothesis (PARMAN *et al.*, 1997; STONE *et al.*, 1987).

The komatiites from the Barberton Mountainland, South Africa are an appropriate focus for a discussion of the role of H_2O in komatiite generation, because the Barberton komatiites have the highest estimated MgO contents of all komatiites. They represent the highest extents of mantle melting and indicate the highest Archean mantle temperatures. The Barberton komatiites are also the Earth's oldest, best-preserved and best exposed komatiites (3.49 Ga, LOPEZ-MARTINEZ *et al.*, 1992). BOYD (1989) proposed that komatiites and depleted Kaapvaal lithosphere might be genetically related. The ages of the melt depletion event recorded in the Kaapvaal harzburgites are comparable to the age of the Barberton komatiites (PEARSON *et al.*, 1995), strengthening the proposal of BOYD (1989).

ESTIMATION OF PRE-ERUPTIVE MAGMATIC H_2O CONTENT

The tools of petrology provide both direct and indirect methods for estimating crystallization conditions. In the case of komatiites, the early estimates of high liquidus temperatures (GREEN *et al.*, 1975) depend on several assumptions: 1) the composition of

the komatiite sample represents the composition of a liquid, 2) the liquid was anhydrous and 3) the liquidus mineral records crystallization conditions. The original estimates of high liquidus temperatures were based assuming that 1) and 2) were true. Assumption 3) could not be fully evaluated, because experimental data on solid -melt exchange for olivine in komatiite melt was not available at the time of the GREEN *et al.* (1975) work.

The solubility of H_2O in silicate melt is extremely pressure sensitive (KUSHIRO and YODER, 1969; HODGES, 1974). At 2 GPa pure forsterite liquid is vapor-saturated when 20 wt. % H_2O is dissolved in the liquid, but H_2O solubility drops to 10 wt. % at 1 GPa, and 0.1 wt. % at 0.1 MPa. Liquids become vapor-saturated as they ascend to crustal pressures and lose their original high pressure magmatic H_2O as the solubility of H_2O drops to nil at surface pressures. The pressure dependence of vapor saturation can eradicate the pre-eruption magmatic H_2O content and result in the preservation of H_2O contents that are lower than the primary value. Olivine is the liquidus phase of komatiite. Dissolved H_2O in silicate melt lowers the olivine liquidus temperature dramatically, but H_2O does not influence Fe-Mg exchange (SISSON and GROVE, 1993; PARMAN *et al.*, 1997). Therefore, the composition of the liquidus olivine provides no direct information on pre-eruptive H_2O content. Crystallization paths and phase appearance sequences are modified by increases in magmatic H_2O, and subliquidus minerals crystallized after hypabyssal emplacement can provide direct evidence of magmatic H_2O. The pyroxenes preserved in Barberton komatiites (PARMAN *et al.*, 1997) and the amphibole found in the Boston Township (STONE *et al.*, 1987) and Munro Township (ARNDT *et al.*, 1977) provide direct evidence of dissolved magmatic H_2O at subliquidus conditions.

Silicate melt inclusions trapped within minerals during crystallization can also provide direct estimates of pre-eruptive volatile contents. In modern subduction-related basalts the H_2O contents of melt inclusions in olivine and pyroxene do record pre-eruptive magmatic H_2O contents (SISSON and LAYNE, 1993) that are in agreement with petrologic estimates. Melt inclusions are abundant in olivine in Barberton komatiites and more rarely preserved in spinel. However, they are invariably serpentinized and consist of the same metamorphic mineral assemblage present in the metamorphosed glassy mesostasis outside of the olivine crystal. Therefore, these meta-melt inclusions only record the bulk composition of the metamorphic mineral assemblage. Even if melt inclusions were preserved, the post crystallization mobility of H_2O in these metamorphic rocks must be critically evaluated in interpreting the water contents of the glasses.

INFLUENCE OF H_2O ON PHASE APPEARANCE AND LIQUIDUS BOUNDARIES

The experimental study of PARMAN *et al.* (1997) provides phase relations for a Barberton komatiite composition at 0.1 MPa, anhydrous and 100 and 200 MPa, H_2O-saturated. The phase relations are summarized in Fig. 1. H_2O lowers the phase appearance temperature for the crystallizing minerals to various degrees. The effect of H_2O on the liquidus temperature (Fig. 1) is inferred from anhydrous and H_2O-saturated experiments on primitive, sub-alkaline basaltic lavas (HAMILTON *et al.*, 1964; SISSON and GROVE, 1993; GAETANI *et al.*, 1994) to be ~80 °C at 200 MPa. The phase appearance temperature of spinel was not directly determined. Experiments on primitive, sub-alkaline basalts (SISSON and GROVE, 1993) show little effect of H_2O on spinel appearance temperature, and this is inferred to be the case for the komatiite composition. The effect of H_2O on the phase appearance temperature of low-Ca pyroxene is dramatic. At 0.1 MPa, a low-Ca pyroxene, pigeonite,

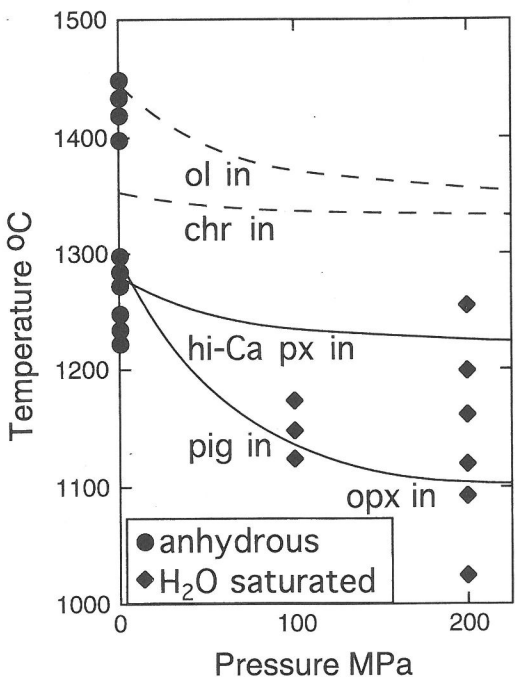

FIG. 1. Phase appearance temperatures at 0.1 MPa (anhydrous) and 100 and 200 MPa (H_2O saturated). Solid circles are 0.1 MPa experiments. Solid diamonds are H_2O-saturated experiments. Note the relatively large effect of H_2O on low-Ca pyroxene stability.

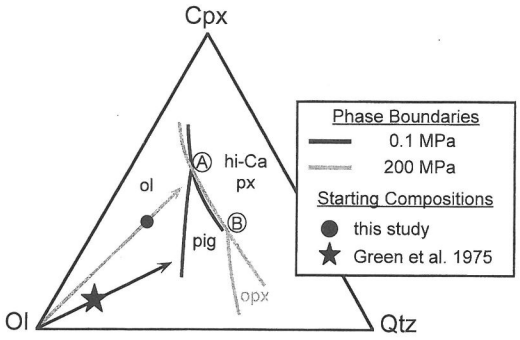

FIG. 2. Compositions of experimental melts with inferred multiple saturation boundaries at 0.1 MPa (anhydrous) and 200 MPa (H_2O saturated). The starting compositions used in this study is shown as a solid black circle. The GREEN *et al.* (1975) composition is shown as the star. The projection scheme is described in GROVE (1993). Arrows show olivine fractionation paths.

appears at 1285°C, while at 200 MPa, a low-Ca pyroxene (now orthopyroxene) appears at ~1100°C. The effect of H_2O content on the appearance temperature of hi-Ca clinopyroxene (hi-Ca pyx) is small (Fig. 1).

Variations in magmatic H_2O affect the phase boundaries and primary phase regions for the Barberton komatiite (Fig. 2). Though simplified into a mineral component representation (GROVE, 1993), this projection scheme illustrates most of the compositional variations for low-Al komatiites, like the Barberton rocks. This phase diagram provides an explanation for the changes in low-Ca and hi-Ca pyroxene phase appearance (Fig. 1) that occur in response to the increase of H_2O in the melt with increasing pressure. The major effect of H_2O in the melt is to expand the olivine liquidus field and to displace the primary liquidus field of low-Ca pyroxene to higher silica contents. The increased H_2O has little effect on the hi-Ca pyx primary phase field or on the position of the olivine + hi-Ca pyx saturation boundary.

KUSHIRO (1969) studied the system forsterite–diopside–silica with and without H_2O and showed that H_2O expands the liquidus field of forsterite at the expense of the enstatite liquidus field. Therefore, increased magmatic H_2O has a similar influence on the olivine and pyroxene primary phase regions in both the simple system forsterite–diopside–silica and the natural komatiite system. KUSHIRO (1973) suggested that the olivine primary phase field expanded because the addition of H_2O broke up polymerized Si – O chains in the melt, thereby favoring crystallization of silicate minerals in which there was less linkage of SiO_4 tetrahedra. Thus, the olivine primary phase field expanded. Another way to think about changes in the behavior of SiO_2 in the melt is to calculate silica activity for the coexistence of pyroxene and olivine. For the reaction,

$$Mg_2Si_2O_{6\ \text{hi-Ca pyx}} = Mg_2SiO_{4\ \text{olivine}} + SiO_{2\ \text{liquid}} \quad (1)$$

the effect of H_2O on silica activity is shown in Fig. 3. GAETANI and GROVE (1998) calculated the influence of H_2O on silica activity in liquids saturated with olivine + orthopyroxene + hi-Ca pyroxene + spinel and found that the influence of H_2O is significant and causes silica to behave more like an ideal component in the melt. In Fig. 3 the calculated ΔG_{rxn} from GROVE and JUSTER (1989, Table, 4, reaction 1b) was used to estimate the value of the equilibrium constant (K) for reaction [1], where

$$K = (a^{oliv}_{Mg2SiO4} * a^{liq}_{SiO2})/(a^{hi\text{-}Ca\ pyx}_{Mg2Si2O6}).$$

Activities were calculated for the olivine and hi-Ca pyx (ANDERSEN *et al.*, 1993) that coexist with liquid in the experiments of PARMAN *et al.* (1997) and used to calculate values for a^{liq}_{SiO2}. The activities of both solids drop by similar amounts. At the same time the

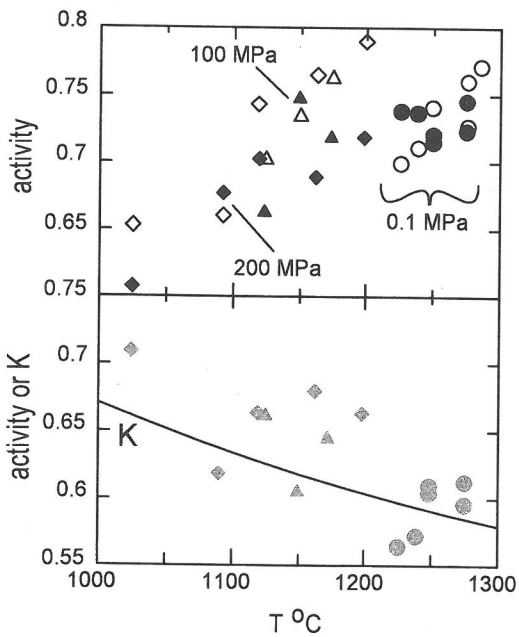

FIG. 3. Calculated activities of minerals and melts from experiments of PARMAN *et al.* (1997). Circles are 0.1 MPa, triangles show 100 MPa and diamonds are 200 MPa experiments. Upper panel shows variation of activity of olivine (open symbols) and hi-Ca pyroxene (solid symbols) calculated using ANDERSEN *et al.* (1993). Lower panel shows variation in value of the equilibrium constant for reaction [1] (solid line) and calculated liquid silica activity (a^{liq}_{SiO2}) for each experiment.

value of K for reaction [1] increases with decreasing temperature. Since the calculated activities for the solids decrease in similar proportion and K increases, a^{liq}_{SiO2} must increase. The expansion of the olivine stability field is caused by the temperature-lowering effect of H_2O. The olivine + pyroxene + melt assemblage is stabilized to lower temperatures, and a^{liq}_{SiO2} is responding to the temperature dependence of the equilibrium constant. A similar effect was noted by GAETANI and GROVE (1998, see their Fig. 5) on the equilibrium constant governing forsterite–liquid equilibria.

These changes in liquidus phase relations exercise important controls on the mineral assemblage that develops in a crystallizing komatiite and on the sequence of phase appearance and liquid line of descent followed by komatiite magmas with varying H_2O content. If a komatiite magma crystallizes at elevated pressures, the mineral assemblage can provide a means of estimating the pre-eruptive magmatic H_2O content.

INFLUENCE OF BULK (STARTING) COMPOSITION ON LIQUID LINE OF DESCENT

Bulk composition of the initial liquid is another key variable in controlling the crystallization sequence followed by a magma. In the case of the Barberton komatiites there is a large variation in major element composition of analyzed rocks (Fig. 4). The rocks span a range from low-SiO_2, low-CaO, high MgO (33 wt. %, recalculated on an anhydrous basis) to high-SiO_2, high-CaO, low-MgO (24 wt. % recalculated on an anhydrous basis). The data set (SMITH *et al.*, 1980; SMITH and ERLANK, 1982) includes only aphyric chill margins. These are the best candidates for liquid compositions. Early discussions on the influence of metamorphism on komatiite bulk composition (GREEN *et al.*, 1975; BESWICK, 1982; SMITH and ERLANK, 1982) concluded that there was only a minor influence. In contrast, DE WIT *et al.* (1987), NISBET *et al.* (1993), and PARMAN *et al.* (1997) show that the H_2O content of the metamorphic rock, major element composition and metamorphic mineral assemblages are correlated. These authors argue that open-system metamorphic exchange between the rock and a metamorphic fluid is responsible for the variation in major elements. Figure 4 illustrates the control of open-system metamorphism on major elements. In the olivine-clinopyroxene-quartz pseudoternary, the compositions of the chill margins vary along a linear trend (Fig. 4). This trend is collinear with the projected compositions of metamorphic serpentine and chlorite minerals found in the rocks. There is also a correlation with H_2O content of

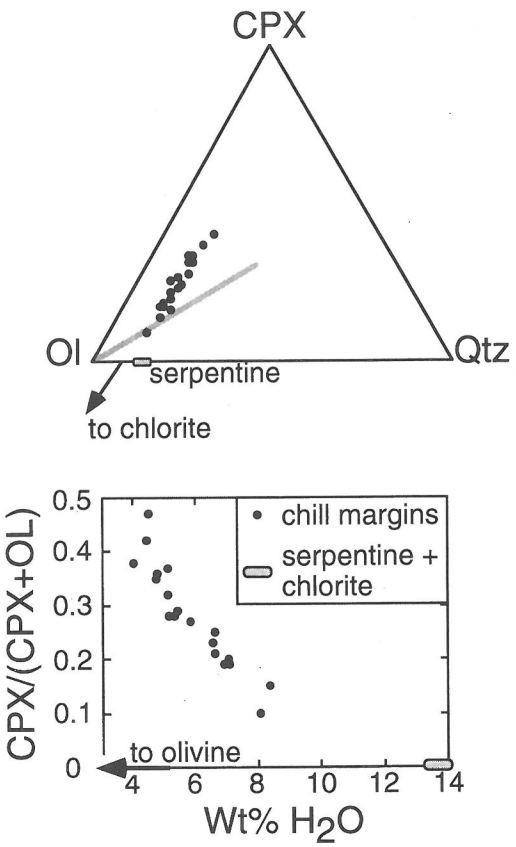

FIG. 4. Upper diagram shows compositions of Barberton komatiite chill margins and aphyric zones projected onto the pseudoternary Oliv-Cpx-Qtz. Data are from SMITH and ERLANK (1980) and SMITH *et al.* (1982). Also indicated are the compositions of the dominant metamorphic minerals in the rocks, serpentine and chlorite. The line indicates the data trend expected if the primary compositional control was olivine fractionation with the most olivine normative rocks being the primitive melts. Lower diagrams shows the compositions of the chill margins projected onto the Ol-Cpx join and plotted against their H_2O content (loss on ignition). The H_2O is hosted in the metamorphic mineral assemblage and therefore represents the extent of alteration.

the metamorphic rock (Fig. 4). The observed compositional variation records an open system reaction whereby primary igneous hi-Ca pyroxene converts to metamorphic tremolite. Continued fluid influx and metamorphic reaction alters the tremolite to serpentine and chlorite, resulting in an increase in MgO and H_2O and a decrease in CaO and SiO_2 of the metamorphic rock. Note that an igneous trend would be expected to be collinear with the liquidus mineral, olivine, if the compositional variation was generated by pre-emplacement fractionation. The observed trend is consistent with a metamorphic process that depleted soluble elements (i.e. Na, Ca, K) from the

rocks, and left behind an MgO-enriched metamorphic assemblage of serpentine and chlorite.

Having identified the igneous protolith for the Barberton komatiites, the effects of variable H_2O on the liquid line of descent can be evaluated. The least altered sample lies at the high-CaO, high-SiO_2 end of the komatiite compositional array. This composition was chosen for experimental study by PARMAN *et al.* (1997) and used to generate the phase diagram (Fig. 2). The composition used by GREEN *et al.* (1975) lies at the extreme high-MgO, low-SiO_2, high-H_2O end of the compositional array of Barberton komatiite chill margins (Fig. 4) and corresponds to the most altered end of the metamorphic array.

Variations in H_2O content influence the liquid line of descent of komatiite magma (Fig. 2). This discussion neglects the influence of Cr-spinel, which appears after olivine and has little influence on the path followed by residual liquids in the Oliv–Cpx–Qtz pseudoternary projection scheme. Under 0.1 MPa anhydrous conditions, the high-CaO, high-SiO_2 composition (BK in Fig. 2) has olivine as its liquidus phase. Olivine crystallization drives the residual liquid toward the olivine - pigeonite reaction boundary where olivine + liquid react to form pigeonite. The liquid moves a short distance along this reaction boundary to the reaction boundary:

olivine + liquid = pigeonite + hi-Ca pyroxene. (A)

The liquid composition will remain at this reaction boundary (under equilibrium conditions) until all liquid is exhausted and the solid assemblage consists of olivine + pigeonite + hi-Ca pyroxene. The 0.1 MPa experiments reported by PARMAN *et al.* (1997) exhibit this behavior. Under conditions of fractional crystallization, olivine would be removed from reaction with liquid, either by crystal settling in the lava flow or by reaction overgrowth of low-Ca pyroxene around olivine. The liquid would leave the reaction boundary and evolve along the pigeonite + augite saturation boundary (dark line in Fig. 2 that extends toward the Qtz apex). At 200 MPa, H_2O-saturated, olivine is again the liquidus phase. Olivine crystallization follows the same path, but because the low-Ca pyx boundary has shifted to higher SiO_2 values, the residual liquid reaches the olivine + hi-Ca pyroxene saturation boundary (grey line in Fig. 2 that parallels the pigeonite + augite boundary). Along this boundary olivine + hi-Ca pyx crystallize and the liquid becomes SiO_2 enriched. After ~60 % crystallization the residual liquid reaches the reaction boundary:

olivine + liquid = orthopyroxene + hi-Ca pyroxene. (B)

Under equilibrium conditions the residual liquid will remain at this boundary until all liquid is exhausted.

Crystallization paths under anhydrous conditions and H_2O-saturated at 200 MPa follow two contrasting phase appearance sequences as a result of the expansion of the olivine and contraction of the low-Ca pyroxene primary phase regions. Under anhydrous conditions, low-Ca pyroxene (pigeonite) appears as the first pyroxene—before hi-Ca pyx. Under H_2O-saturated conditions hi-Ca pyx appears first, and crystallizes for a significant temperature interval (~100°C). If one considers the crystallization path followed by a low-SiO_2, high-MgO composition (*e.g.*, the GREEN *et al.* [1975] composition) a distinctively different crystallization sequence would be inferred. Under anhydrous 0.1 MPa conditions, pigeonite would again be the first low-Ca pyroxene to crystallize, but it would crystallize in reaction relation along the olivine - pigeonite reaction boundary. Under conditions of fractional crystallization pigeonite crystallizes and the liquid enters the pigeonite primary phase region. Crystallization continues over a significant temperature interval (>100°C) before hi-Ca pyroxene joins the crystallizing assemblage. In the case of 200 MPa H_2O-saturated conditions, olivine would crystallize over a larger temperature interval, and augite + orthopyroxene would appear simultaneously at the 200 MPa reaction boundary (B). Therefore, the pyroxene assemblages in a komatiite provide information to infer variations in crystallization conditions (anhydrous vs hydrous). If there is a variation in parental magma compositions, the mineral assemblages in each contrasting composition should be consistent with the composition of the rock relative to the phase boundaries. In the case of Barberton komatiites, high-MgO anhydrous komatiites should contain abundant pigeonite.

Only a hi-Ca pyx is present in the olivine komatiites from the lower part of the Komati Formation. These units are inferred to form by crystallization of near H_2O-saturated magmas with ~6 wt. % H_2O and are interpreted as sills emplaced at ~6 km depth (see next section). PARMAN *et al.* (1997) also find evidence for variable crystallization conditions of a parent magma similar to the high-CaO, high-SiO_2 composition (BK). Komatiites in the upper Komati Formation contain pigeonite cores overgrown by augite rims (GROVE *et al.*, 1997, Fig. 4.4.2.10 and PARMAN *et al.*, 1997, Fig. 6). This assemblage indicates that these komatiite magmas contained less H_2O than the melt that produced the olivine spinifex komatiites in the lower Komati Formation. If an initially hydrous komatiite magma was emplaced at shallow levels, the sharp decrease in H_2O solubility with depth would

lead to vapor saturation, degassing of H_2O and anhydrous crystallization that produced early pigeonite.

Influence of H_2O on mineral compositions

H_2O also influences the composition of the pyroxene that crystallizes. The compositional effects are primarily related to the lower temperature at which pyroxene and melt coexist. Pyroxene Wo (Wo = $CaSiO_3$) contents in the 200 MPa, H_2O saturated experiments are distinctly higher than the pyroxene Wo contents in the 0.1 MPa experiments (Fig. 5). High Wo contents are recognized as a characteristic of clinopyroxene crystallized from hydrous melts (SISSON and GROVE, 1993; GAETANI *et al.*, 1994). The lowered crystallization temperature of the hi-Ca pyroxene causes higher Wo contents, because the two-phase region (augite - orthopyroxene) expands as temperature drops. The magnitude of the thermodynamic non-ideality in the hi-Ca pyroxene is temperature dependent. At lower temperatures the non-ideal term is relatively larger (LINDSLEY *et al.*, 1981). Therefore, phase compositions are closer to end member compositions. Even when the augite is not saturated with a low-Ca pyroxene, the non-ideality is

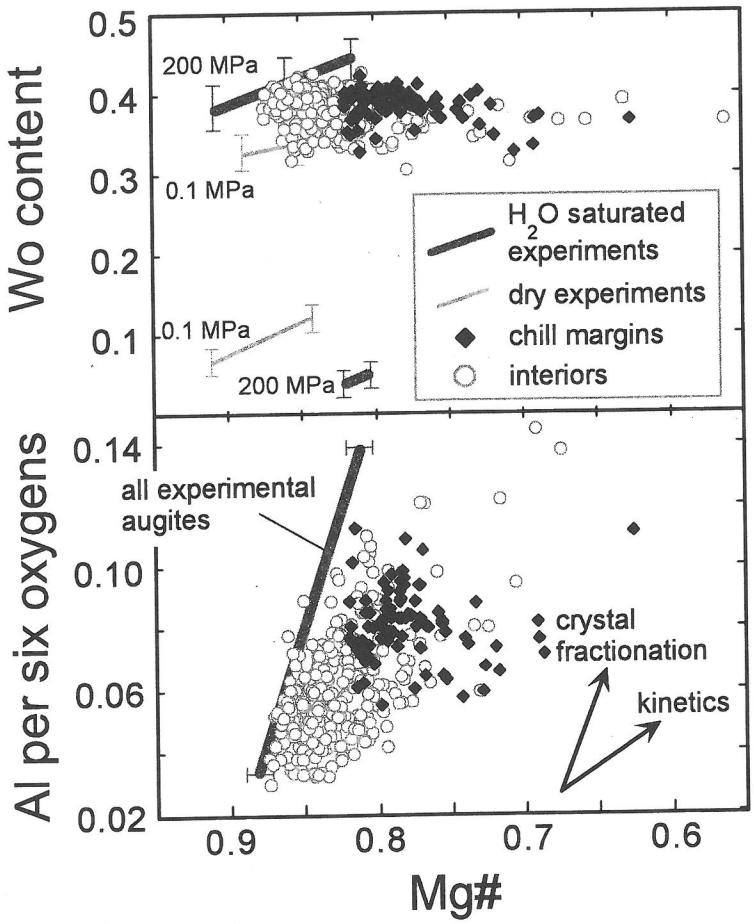

FIG. 5. Upper figure shows wollastonite (Wo) content versus Mg# in hi-Ca pyx in chill margins (solid diamonds) and interiors of units (open grey circles). Lines show compositions of pyroxenes produced in 0.1 MPa, anhydrous experiments (light grey) and 200 MPa, H_2O saturated experiments (dark grey) from PARMAN *et al.* (1997). Error bars show range of pyroxene compositions. The highest Mg# points are the cores of crystals. These are first pyroxene crystals to form and they are interpreted to record the emplacement conditions. Note the good correspondence between the cores of augite from the interior of the units and the 200 MPa H_2O-saturated experimental data. Lower figure shows Al per six oxygens versus Mg# for natural and experimental augite. Both sets of experimental data are similar in Al content, with the 0.1 MPa data falling on the low side of the range. Augite cores from chill margins fall off the experimental trend because of their delayed nucleation and the effect of cooling rate on partitioning.

still present, causing higher Wo contents. The effect of increasing H_2O in the melt stabilizes melt, pyroxene and olivine to lower temperature. The activities of the $(Fe,Mg)SiO_3$ components in the hi-Ca pyx decrease with temperature (Fig. 3), which leads to an increase in the $CaSiO_3$ component in the hi-Ca pyroxene that coexists with olivine and melt.

In comparison, the pyroxene compositions produced in the 0.1 MPa anhydrous experiments record higher temperatures (~25 °C) for the coexistence of the first pigeonite and augite pair to crystallize. The Ca contents of the augite are lower, because the pigeonite–augite miscibility gap is narrow at these higher temperatures compared to the orthopyroxene–augite two-phase region. Pressure has a negligible effect on the phase relations (LINDSLEY and ANDERSEN, 1983). The main effect of increased pressure alone is to lower the Wo content of the augites by raising the temperature at which they crystallize under anhydrous conditions.

INFLUENCE OF COOLING RATE—CRYSTALLIZATION KINETICS ON MINERAL COMPOSITIONS

In the Komati Formation, the cooling units that have been studied are on the order of 1 to 55 meters thick. The results of isothermal crystallization experiments discussed above are relevant to the slowly cooled interiors of the thicker units. It is important to determine the range of cooling rates where kinetic effects may influence the appearance sequence and composition of crystallizing phases. PARMAN *et al.* (1997) performed cooling rate experiments on the BK composition at 3 and 10°C/hour. These cooling rates would correspond to distances of 0.5 and 0.2 m, respectively, from a boundary of conductive heat loss in a cooling Barberton komatiite sill. In the cooling rate experiments, textures indicate that olivine is the liquidus phase, followed by spinel and then followed by pigeonite and augite. The effect of cooling rate is to suppress the appearance temperature of later phases, specifically pigeonite and augite (PARMAN *et al.*, 1997).

Textural evidence in the experiments indicates that faster cooling rates suppress pigeonite crystallization more than augite crystallization. In the 10°C/hr experiment the pigeonite cores are very small and constitute <5 volume % of the crystal. At cooling rates faster than 10°C/hr, pigeonite does not crystallize, a result in accordance with the work of KINZLER and GROVE (1985). KINZLER and GROVE (1985) also found that increased cooling rate suppresses the nucleation of pigeonite relative to augite. This relative suppression of pigeonite in the cooling rate experiments is a result of crystal/melt disequilibrium. Increased cooling rate increases crystal growth rates and the lower temperature results in a decrease in melt diffusion rates. Diffusion in the melt is not rapid enough to remove elements from or supply them to the advancing crystal face. Crystals are forced to grow from a melt with higher concentrations of incompatible elements and lower concentrations of compatible elements. Therefore, as cooling rates increase, partition coefficients converge on a value of unity. So, the composition of the pyroxene becomes increasingly similar to the melt. Augite is closer in composition to the melt than pigeonite and, therefore, is relatively more stable in the disequilibrium system. Therefore the increased disequilibrium at fast cooling rates favors the nucleation of augite over pigeonite.

The chill margins of Barberton olivine spinifex komatiite units contain fresh hi-Ca pyroxene (Fig. 5). The pyroxene compositions reflect the rapid cooling rates at the chill margin. The composition of the first pyroxene to crystallize has lower Wo content and Mg# and higher Al contents than the first pyroxene that crystallized in the slowly cooled interiors of the units or in the 200 MPa isothermal experiments. The major and minor element compositions of the pyroxenes from the slowly cooled interiors do not show the effects of rapid cooling rate. The compositions of the cores of the pyroxenes from the slowly cooled interiors are nearly identical to the pyroxenes produced in the isothermal experiments of PARMAN *et al.* (1997). Therefore, the effect of cooling rate is negligible in the interiors of the units, and we can use the compositions of the pyroxenes in the isothermal experiments to infer emplacement conditions.

INTERPRETING THE MINERALOGICAL EVIDENCE IN OTHER KOMATIITES

ARNDT *et al.* (1998) equate the compositions of pyroxenes produced in rapidly chilled margins in the komatiites of the Munro Township to those produced in the isothermal experiments of PARMAN *et al.* (1997). The hi-Ca augites with high Al_2O_3 contents in the chill margins of Munro Township komatiites are not compositionally similar to the PARMAN *et al.* (1997) isothermally produced low-Al augites. A quick comparison of minor element compositions shows that these Munro pyroxenes contain from 7.8 to 8.5 wt. % Al_2O_3. In contrast, the pyroxenes in the Barberton komatiites and the PARMAN *et al.* (1997) experiments contain 1 to 1.5 wt. % Al_2O_3. KINZLER and GROVE (1985) produced high-Al pyroxenes similar to those found in the Munro samples in rapid cooling rate experiments and discuss the near surface origin for the Munro Township pyroxenes.

Other Archean komatiite localities have features that point to variations in the H_2O content of the crystallizing komatiite magma. In the Munro Township locality (PYKE *et al.*, 1973) olivine spinifex komatiites at Pyke's hill contain early crystallizing pigeonite (ARNDT *et al.*, 1977), permissive evidence for anhydrous crystallization at near surface conditions. However, thick differentiated sills, also present in the Munro Township, contain igneous amphibole. Amphibole is an important indicator of the presence of significant quantities of magmatic H_2O (>2 wt. % H_2O at the minimum pressure of amphibole stability). The thick, differentiated units (like Fred's Flow, ARNDT *et al.*, 1977) and other late Archean komatiites in the Abitibi belt (Boston Township, STONE *et al.*, 1987) are likely to be intrusive. As a consequence of their higher pressure of emplacement, they record a higher pre-eruptive H_2O content. However, rather than generalize the results from Barberton to all komatiites, a careful re-evaluation of the petrologic evidence for the role of H_2O in komatiitic magmatism is needed.

PRE-ERUPTIVE H_2O CONTENTS IN MODERN BASALTIC MAGMAS

Komatiites are found predominantly in Archean and early Proterozoic greenstone belts. The Tertiary Gorgona Island komatiites (ECHEVERRIA, 1980) are the closest Phanerozoic analogs to komatiites. The pre-eruptive H_2O contents for these rocks have not been quantitatively investigated, but there is an interesting association of ultramafic tuff with the komatiite units (ECHEVERRIA, 1980). Modern primitive magmas with H_2O contents similar to those inferred for Barberton komatiites (4–6 wt. % H_2O) are present in subduction zone environments. ANDERSON (1979) and BAKER *et al.* (1994) report primitive basaltic andesite (10.5 wt. % MgO) and andesite (9.1 wt. % MgO) from the Southern USA Cascades that contain 4.5 to 6.5 wt. % H_2O. Primitive basaltic rocks from the Oregon and Washington Cascades contain ~4 wt. % H_2O (CONREY *et al.* 1997). MOORE and CARMICHAEL (1998) use evidence from the compositions of phenocrysts preserved in Mexican basaltic andesites to infer pre-eruptive H_2O contents of ~6 wt. %. Thus, in modern environments, high-H_2O primitive magmas are found in subduction zone settings. By analogy a possible Archean environment for the production of hydrous komatiites is in a subduction-related setting. In the final section we develop a model for melt production in an Archean subduction setting.

Another factor must be considered in comparing magmas from modern subduction zones with those found in Archean Greenstone Belts. Petrologic evidence indicates production of melts of widely varying H_2O content closely related in space and time (BAKER *et al.*, 1994). Such complexities could also exist in the komatiite melt generation regime. Careful field studies and detailed petrologic examination will be required to infer the conditions recorded in these important ancient igneous rocks.

IMPLICATIONS OF ELEVATED PRE-ERUPTIVE H_2O CONTENTS FOR ARCHEAN MANTLE CONDITIONS

Experiments

Previous high pressure experimental studies on komatiites have investigated the conditions of anhydrous mantle melting that could lead to the production of komatiite magmas (GREEN *et al.*, 1975; HERZBERG, 1989). We used the pre-eruptive H_2O content estimate of PARMAN *et al.* (1997) to investigate the influence of H_2O on the high pressure phase relations of a primitive 24 wt. % MgO Barberton komatiite. The liquidus phase relations are shown in Fig. 6, and experimental conditions are provided in Table 1. The purpose of these experiments is to provide constraints on the conditions for melt generation in the mantle source of Barberton komatiites.

Experimental methods. The experiments were performed in a piston cylinder apparatus (BOYD and ENGLAND, 1960) over the pressure range of 2.0 to 2.5 GPa. The pressure medium consisted of sintered $BaCO_3$, and pressure was calibrated using the Ca-Tschermakite reaction (HAYS, 1966). Temperature was monitored and controlled using $W_{97}Re_3$-$W_{75}Re_{25}$ thermocouples, and no correction for the effect of pressure on thermocouple EMF was applied. The sample was positioned in the hot spot of the experimental assembly. The temperature difference between the sample

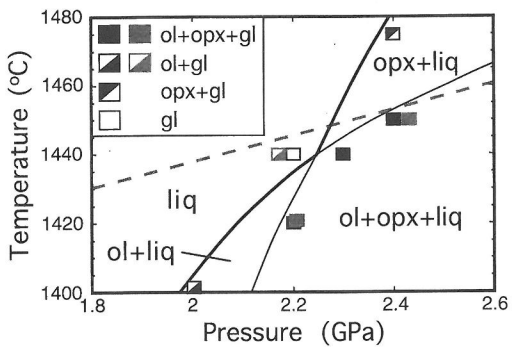

FIG. 6. Melting experiments carried out on the least altered Barberton komatiite composition of PARMAN *et al.* (1997) containing 6 wt. % H_2O. Black squares show experiments in unsaturated $Au_{80}Pd_{20}$ capsules. Grey squares show experiments in Fe-saturated capsules. The dashed line is the inferred melting point of the Fe-saturated $Au_{80}Pd_{20}$. Failed (capsule melted) experiments were used to define the capsule melting boundary, and these are omitted from the diagram Other lines are phase stability fields inferred from experiments.

Table 1. Conditions and results of elevated pressure experiments on Barberton komatiite composition BK.

Expt. #	Pressure (GPa)	T (°C)	time (hours)	Phases[1]	wt. % Fe in capsule	% Fe loss/gain	K_D[2] ol/liq	K_D opx/liq
BK2.2	2.0	1400	7	q, ol	0.0	-	0.3	
BK2.3	2.4	1450	9	q, ol, opx	0.0	na[3]		
BK2.4	2.4	1475	8	q, opx	0.0	-13		0.29
BK2.5	2.2	1440	6	g, ql	0.0	-8		
BK2.6	2.25	1420	7.5	q, ol, opx	0.0	-5	0.27	0.25
BK2.7	2.3	1440	4.5	q, ol, opx	0.0	-8	0.29	0.26
BK2.9	2.2	1420	21	q, ol, opx	1.35	+10	0.32	0.29
BK2.12	2.2	1440	6	q, ol	0.94	+11	0.30	
BK2.15	2.4	1450	8	q, ol, opx	0.67	+10	0.35	0.30

[1] Abbreviations: q = quench crystals from liquid, gl = quenched glass, ol = olivine, opx = orthopyroxene.
[2] $K_D = [(X_{Fe}^{xtal} * X_{Mg}^{liq})/(X_{Mg}^{xtal} * X_{Fe}^{liq})]$
[3] na = not analyzed.

and thermocouple was measured, and a 20 °C correction was applied.

The starting composition is a synthetic analog of the least altered Barberton komatiite chill margin used by PARMAN *et al.* (1997). The starting composition was fabricated using oxide starting materials following the technique described in GAETANI and GROVE (1998). In order to add H_2O to the starting material, a portion of the MgO was added as brucite and the remainder was added as anhydrous MgO (BAKER *et al.*, 1994). The resulting starting mix contained 6 wt. % H_2O. Approximately 10 to 15 mg of starting material was loaded into $Au_{80}Pd_{20}$ capsules that were welded shut. The Au-Pd alloy capsule was placed into an MgO sleeve. This assembly was placed into an outer Pt capsule, packed with MgO at both ends and welded shut. The experimental conditions were very close to the melting point of the Au-Pd alloys. We initially used capsules that had been pre-saturated with Fe to minimize Fe exchange between the sample and container (GAETANI and GROVE, 1998), but some of these melted in our experiments. Figure 6 shows the solidus of the $Au_{80}Pd_{20}$ alloy as determined during the course of the experiments. In order to determine the liquidus of the Barberton komatiite, some unsaturated $Au_{80}Pd_{20}$ capsules were used.

Experimental products were analyzed using the JEOL 4- or 5- spectrometer electron microprobe at MIT. Liquids in these experiments did not quench to glass and consist of micron-sized quench pyroxene crystals set in glass. This quench growth was analyzed using a broad electron microprobe beam (30 microns), and 20 to 30 replicate analyses of the glass phase were used to obtain an estimate of melt composition. Crystalline phases (olivine and orthopyroxene) were analyzed using a 2 micron beam. The values of Fe-Mg exchange distribution coefficients $(K_D^{Fe\text{-}Mg}) = [(X_{Fe}^{xtal} * X_{Mg}^{liq})/(X_{Mg}^{xtal} * X_{Fe}^{liq})]$ for olivine–melt and orthopyroxene–melt are provided in Table 1 and are comparable to the values obtained in other elevated pressure experimental studies of basaltic compositions (*e.g.*, KINZLER, 1997). The calculated gain or loss of Fe from the silicate charge to the $Au_{80}Pd_{20}$ capsule is also shown. All of the experiments either lost or gained from 5 to 10 wt. % FeO. Although such changes in composition of the silicate portion of the charge are not desirable, the results of these experiments are judged to provide a reasonable approximation of the liquidus phase relations, for the following reasons. 1) We duplicated several of the lower temperature experiments using Fe-doped and undoped capsules to see whether there was a change in the phase relations (Table 1). The results were similar. 2) The Fe-Mg K_D's for olivine and orthopyroxene achieved the same value in doped and undoped capsules. Therefore, exchange equilibrium for these elements between melt and solid was achieved in the experiments. For these reasons the phase diagram presented in Fig. 6 is thought to be an accurate representation of a komatiite liquid containing 6 wt. % H_2O.

Experimental results. With 6% H_2O the Barberton composition is multiply saturated with olivine and orthopyroxene on its liquidus at 2.2 GPa and 1430°C (Fig. 6). This multiple saturation point is equivalent to a melt residue of harzburgite. Thus, the melt segregated after high extents of melting. In contrast, HERZBERG (1992) concluded that Barberton komatiites similar to the composition studied by GREEN *et al.* (1975) were derived from deep sources (260 to 330 km depth) from a residue consisting of olivine, garnet and subcalcic augite at a temperature of 1800 to 2000 °C.

Models for komatiite melting

Early anhydrous models for komatiite generation assumed that the experimentally determined multiple saturation point represented the depth and temperature of melt segregation. Thus, melting was modeled as a batch process. A near fractional adiabatic decompression melting model was described by HERZBERG (1995). His proposed adiabatic melting path uses an estimate of the maximum depth of melting from petrologic criteria (CaO/Al_2O_3 of the melt) and the melting path starts at >300 km depth. Estimates of the amount of melt produced during decompression melting $[(dF/dP)_S]$ range from about 1 to 3 wt. %

per 0.1 GPa. (AHERN and TURCOTTE, 1979; MCKENZIE, 1984; KINZLER and GROVE, 1992). If these melting rates are applied to the HERZBERG (1995) dry melting path, only a part of the adiabatic ascent path is necessary to generate a sufficient melt fraction to produce a komatiite magma as a partial melt from a primitive mantle (~50% melting). HERZBERG (1995) does not discuss what conditions or mechanisms would lead to a cessation of melting. A drawback of this melting model is that melting begins in a depth region where the ultramafic partial melt would be more dense than its surrounding solid mantle residue (AGEE and WALKER, 1993), and melt would sink rather than ascend.

For hydrous decompression melting, a near-fractional melt generation process is not feasible. Near-fractional melting models assume that once a melt batch is produced, it is removed and no longer interacts with the mantle. All the H_2O would be removed with the first melt fraction. Subsequent fractional melts would have to be generated under anhydrous conditions, which would require a large increase in temperature. Such a process does not seem relevant to the generation of hydrous komatiite magmas. Magmatic H_2O could be retained in a batch melting process. In the case of hydrous batch melting, the crystalline residue and melt ascend together and constantly re-equilibrate as melting proceeds. Once the melt is removed, it would retain the signature of the last temperature and pressure of equilibration. Another process that could resemble batch melting is flux melting. In this process the H_2O-bearing melt separates from its residue and ascends through the mantle by porous flow. The melt continuously reacts and requilibrates with shallower mantle as it ascends and is subjected to changing pressure and temperature conditions.

If a komatiite magma containing 6% H_2O is generated by high extents of partial melting of a fertile peridotite source (~50% melting) the source must contain 3 wt. % H_2O. There are no hydrous mantle minerals that would be present in sufficient modal abundance to provide the required H_2O. The only other source of H_2O is as free water released by the breakdown of hydrous minerals in the subducting lithosphere. SCHMIDT and POLI (1998) show that dehydration of the downgoing hydrated mantle and slab occurs over a broad range of depths, beginning at 70 km with amphibole breakdown. Dehydration of serpentine and chlorite brings mineralogically bound H_2O to depths of 150 to 200 km, and other dehydration reactions can extend the depth of H_2O release to ~300 km. The H_2O is released, ascends into the overlying mantle wedge and encounters an inverted temperature gradient. When the H_2O-rich fluid reaches mantle that is at the temperature and pressure conditions of the vapor-saturated solidus, an H_2O-rich melt is produced and melting begins. Figure 7 shows a mantle solidus calculated using the approach of KINZLER and GROVE (1992) and including the hydrous mantle melting experiments of GAETANI and GROVE (1998). Also shown is a schematic cross section of the mantle wedge with isotherms and two possible ascent paths for the fluid. If a flux melting process is operative, it can occur when partial melting

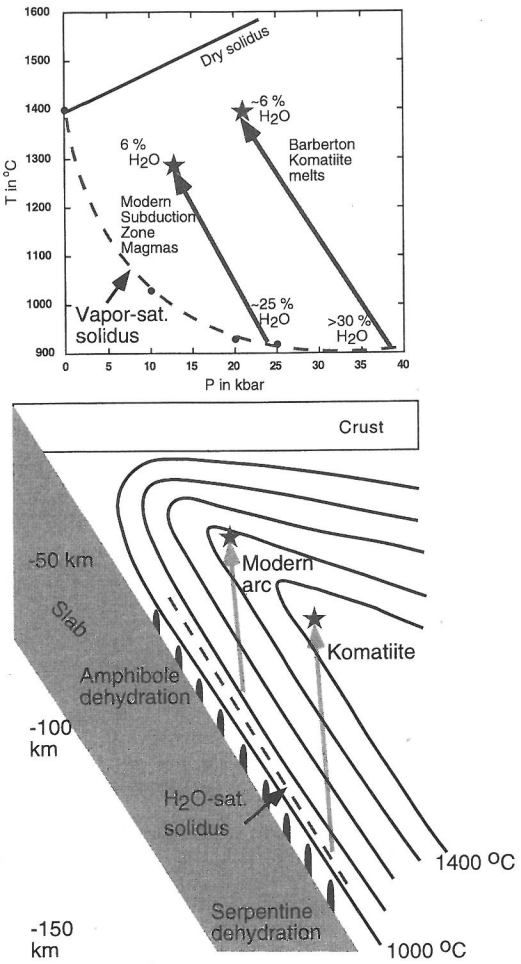

FIG. 7. Subduction zone model for Barberton komatiite production. Top figure is a P–T diagram showing the solidus temperature for dry (solid black line) and H_2O saturated (dashed grey line) peridotite. Arrows connect experimentally determined olivine + orthopyroxene saturation points (stars) for Barberton komatiites and modern high-Mg basaltic andesites with their initial melting conditions at the H_2O-saturated peridotite solidus. Lower figure is a cross-section of a subduction zone comparing melting path for Barberton komatiites with modern arc volcanism. Arrows and stars correspond to P–T conditions in upper figure.

creates an interconnected melt network and an equilibrium melt fraction. When the critical melt fraction is exceeded, this melt segregates from its residue and rises into shallower, hotter mantle. The melt reacts with this mantle, producing additional melt and diluting its H_2O content. As the hydrous melt ascends, it is continuously superheated. If the melt resides in the interconnected network of grain boundaries, it constitutes only a small fraction of the total mass. Therefore, the heat of fusion and specific heat can be supplied from the surrounding solids without lowering the temperature of the mantle. As melt rises and interacts with surrounding mantle, it follows the H_2O-undersaturated liquidus boundary in the natural peridotite–water system. Melting ceases when the normal temperature–depth gradient is encountered. Melt production is controlled by the slope of this boundary and by the temperature–depth conditions of ascent. The melting process is essentially a batch process, because the melt reacts with its surroundings at each step of the process. When the final melt is extracted and delivered to the surface, it would record the final pressure and temperature of equilibration conditions. In the case of the Barberton komatiites this would be the multiple saturation point shown in Fig. 6. The pressure of multiple saturation (2.2 GPa) corresponds to a depth of ~65 km, which is well within a possible depth range for wedge melting in a subduction zone. The temperature of multiple saturation (1430 °C) is at the upper limit of the range of predicted mantle temperatures in thermal models of subduction zones (FURUKAWA, 1993).

The flux melting model for hydrous komatiite operates over a depth interval of about 60 km in the lower part of the wedge (Fig. 7). The combined effects of increasing temperature, decreasing pressure and decreasing H_2O on the phase boundaries will control melting rate. Using existing data to infer melt extent over a pressure change equivalent to 60 km depth, the hydrous flux melting model encounters difficulty. The GAETANI and GROVE (1998) estimate of $(dF/dP)_S$ for mantle melting in the presence of H_2O would predict ~20 wt. % melting over a 60 km depth interval. This contrasts with the ~50 wt. % melt extent that would be inferred for melting of a primitive mantle source. The difficulty can be overcome, if the mantle source of komatiite had been previously depleted by prior melt extraction events. Two possibilities are: prior melt extraction at a spreading center or progressive depletion of the mantle wedge by hydrous flux melting. In the first scenario, melt depletion took place at an Archean mid-ocean or back-arc spreading center, and the depleted mantle was subducted into the wedge. In the second model the komatiite represents the last product of a series of flux melting events experienced by the mantle wedge. Earlier hydrous flux melting of the wedge produces basaltic magmas and depletes the source in high-Ca clinopyroxene and/or garnet. H_2O continues to ascend through the depleted mantle, initiates hydrous melting and the komatiite is the last magma produced and extracted from the depleted source region.

An important geologic constraint is that the komatiites are a small fraction of the mafic–ultramafic section at Barberton and constitute ~10% by volume. As intrusions the komatiites follow emplacement of a 5 to 6 km accumulation of basalts and komatiitic basalts. The magmatic stratigraphy is consistent with the komatiites as the last product of hydrous flux melting.

If the subduction zone hypothesis is the correct interpretation of the komatiite phase relations, then it implies different conditions in subduction zone melt generation during the Archean and Early Proterozoic. The melts produced in modern subduction zones (BAKER *et al.*, 1994) have comparable H_2O contents, but are derived from shallower depths (30 to 45 km) at lower temperatures (1200–1300°C). The difference may be related to the vigor of Archean subduction or to the higher temperatures in the Archean mantle wedge, or both. Back-arc magmatism may have more efficiently depleted the mantle that was fed into Archean subduction zones. Hydrothermal alteration systems at mid-ocean or back-arc spreading centers may have been more active and basalt and mantle may have experienced more extensive hydration prior to subduction. These processes would lead to an increase in the amount of H_2O that was subducted and the depth to which it was subducted. The combination of these factors led to the unique hydrous magmatism preserved in Barberton komatiites.

Acknowledgements—The authors thank Y.Zhang and G. Gaetani for reviews of the paper. The field work benefited greatly from the assistance and support of H. Marais. This work was supported by NSF (USA) and FRD (South Africa).

REFERENCES

AGEE C. B. and WALKER D. (1993) Olivine flotation in mantle melt. *Earth Planet. Sci. Lett.* **114,** 315–324.

AHERN J. L. and TURCOTTE D. L. (1979) Magma migration beneath an ocean ridge. *Earth Planet. Sci. Lett.* **45,** 115–122.

ALLEGRE C. A. (1982) Genesis of Archean komatiites in a wet ultramafic subducted plate. In *Komatiites,* (eds. N. T. ARNDT and E. G. NISBET), pp. 495–500, George Allen & Unwin.

ANDERSEN D. J., LINDSLEY D. H., and DAVIDSON P. M. (1993) QUILF: A Pascal program to assess equilibria

among Fe-Mg-Mn-Ti oxides, pyroxene, olivine and quartz. *Computers Geosci.* **19,** 1333–1350.

ANDERSON A. T., JR. (1979) Water in some hypersthenic magmas. *J. Geol.* **87,** 509–531.

ARNDT N. T. and NISBET E. G. (1982) What is a komatiite? In *Komatiites,* (eds. N. T. ARNDT and E. G. NISBET), pp. 19–27, George Allen & Unwin.

ARNDT N. T., NALDRETT A. J., and PYKE D. R. (1977) Komatiitic and iron-rich tholeiitic lavas of Munro Township, northeast Ontario. *J. Petrol.* **18,** 319–369.

ARNDT N. T., GINIBRE C., CHAUVEL C., ALBAREDE F., CHEADLE M., HERZBERG C., JENNER G., and LAHAYE Y. (1998) Were komatiites wet? *Geology* **26,** 739–742.

BAKER M. B., GROVE T. L., and PRICE R. (1994) Primitive basalts and andesites from the Mt. Shasta region, N. California: products of varying melt fraction and water content. *Contrib. Mineral. Petrol.* **118,** 111–129.

BOYD F. R. (1989) Compositional distinction between oceanic and cratonic lithosphere. *Earth Planet. Sci. Lett.* **96,** 15–26.

BOYD F. R. and ENGLAND J. L. (1960) Apparatus for phase equilibrium measurements at pressures up to 50 kilobars and temperatures up to 1750°C. *J. Geophys. Res.* **65,** 741–748.

CONREY R. M., SHERROD D. R., HOOPER P. R., and SWANSON D. A. (1997) Diverse primitive magmas in the Cascade arc, northern Oregon and southern Washington. *Canad. Mineral.* **35,** 367–396.

DE WIT M. J., HART R. A., and HART R. J. (1987) The Jamestown Ophiolite Complex, Barberton mountain belt: a section through 3.5 Ga oceanic crust. *J. Afr. Earth Sci.* **6,** 681–730.

ECHEVERRIA L. M. (1980) Tertiary or Mesozoic komatiites from Gorgona Island, Colombia: Field relations and geochemistry. *Contrib. Mineral. Petrol.* **73,** 253–266.

FURUKAWA Y. (1993) Magmatic processes under arcs and formation of the volcanic front. *J. Geophys. Res.* **98,** 8309–8319.

GAETANI G. A., GROVE T. L., and BRYAN W. B. (1993) Influence of water on the petrogenesis of subduction-related igneous rocks. *Nature* **365,** 332–334.

GAETANI G. A., GROVE T. L., and BRYAN W. B. (1994) Experimental phase relations of basaltic andesite from Hole 839B under hydrous and anhydrous conditions. *Proc Ocean Drilling Prog.* **135,** 557–563.

GAETANI G. A. and GROVE T. L. (1998) The influence of water on melting of mantle peridotite. *Contrib. Mineral. Petrol.* **131,** 323–346.

GREEN D. H., NICHOLLS I. A., VILJOEN M., and VILJOEN R. (1975) Experimental demonstration of the existence of peridotitic liquids in earliest Archean magmatism. *Geology* **3,** 11–14.

GROVE T. L. (1993) Corrections to expressions for calculating mineral components in "Origin of calc-alkaline series lavas at Medicine Lake volcano by fractionation, assimilation and mixing" and "Experimental petrology of normal MORB near the Kane Fracture Zone, 22–25 °N, mid-Atlantic ridge." *Contrib. Mineral. Petrol.* **114,** 422–424.

GROVE T. L. and JUSTER T. C. (1989) Experimental investigations of low-Ca pyroxene stability and olivine–pyroxene–liquid equilibria at 1 – atm in natural basaltic and andesitic liquids. *Contrib. Mineral. Petrol.* **103,** 287–305.

GROVE T. L., DE WIT M. J., AND DANN J. C. (1997) Komatiites from the Komati type section, South Africa, In *Greenstone Belts,* (eds. M. J. DE WIT and L. D. ASHWAL), pp. 435–450, Oxford University Press.

HAMILTON D. L., BURNHAM C. W., and OSBORN E. F. (1964) The solubility of water and the effects of oxygen fugacity and water content on crystallization in mafic magmas. *J. Petrol.* **5,** 21–39.

HAYS J. F. (1966) Lime-alumina-silica. *Carnegie Inst. Wash. Yrbk.* **65,** 234–239.

HERZBERG C. (1992) Depth and degree of melting of komatiites. *J. Geophys. Res.* **97,** 4521–4540.

HERZBERG C. (1995) Generation of plume magmas through time: an experimental perspective. *Chem. Geol.* **126,** 1–16.

HODGES F. N. (1974) Solubility of H_2O in forsterite melt at 20 kbar. *Carnegie Inst. Wash. Yrbk.* **72,** 495–497.

KINZLER R. J. (1997) Melting of mantle peridotite at pressures approaching the spinel to garnet transition: Application to mid-ocean ridge basalt petrogenesis. *J. Geophys. Res.* **102,** 853–874.

KINZLER R. J. and GROVE T. L. (1985) Crystallization and differentiation of Archean komatiite lavas from northeast Ontario: phase equilibrium and kinetic studies. *Amer. Mineral.* **70,** 40–51.

KINZLER R. J. and GROVE T. L. (1992) Primary magmas of mid-ocean ridge basalts 1: Experiments and Methods, 2: Applications. *J. Geophys. Res.* **97,** 6885–6926.

KUSHIRO I. (1969) The system forsterite-diopside-silica with and without water at high pressures. *Amer. J. Sci.* **267A,** 269–294.

KUSHIRO I. (1973) Regularities in the shift of liquidus boundaries in silicate systems and their significance in magma genesis. *Carnegie Inst. Wash. Yrbk.* **72,** 497–502.

KUSHIRO I. and YODER H. S. JR. (1969) Melting of forsterite and enstatite at high pressures under hydrous conditions. *Carnegie Inst. Wash. Yrbk.* **67,** 153–158.

LINDSLEY D. H. and ANDERSEN D. J. (1983) A two pyroxene thermometer. *Proc 13th Lunar Planet. Sci. Conf., Part 2,* A887–A906.

LINDSLEY D. H., GROVER J. E., and DAVIDSON P. M. (1981) The thermodynamics of the MgSiO3 - CaMgSi2O6 join: A review and an improved model. In *Thermodynamics of Minerals and Melts, v. 1* (eds. R. C. NEWTON, A. NAVROTSKY and B. J. WOOD), pp. 149–175, Springer-Verlag.

LOPEZ-MARTINEZ M., YORK D., and HANES J. A. (1992) A 40Ar/39Ar geochronological study of komatiites and komatiitic basalts from the Lower Onverwacht Volcanics: Barberton Mountainland, South Africa. *Precambrian Res.* **57,** 91–119.

MCKENZIE D. (1984) The generation and compaction of partially molten rock. *J. Petrol.* **25,** 713–765.

MOORE G. and CARMICHAEL I. S. E. (1998) The hydrous phase equilibria (to 3 kbar) of an andesite and basaltic andesite from western Mexico: constraints on water content and conditions of phenocryst growth. *Contrib. Mineral. Petrol.* **130,** 304–319.

NISBET E. G., CHEADLE M. J., ARNDT N. T., and BICKLE M. J. (1993) Constraining the potential temperature of the Archaean mantle: A review of the evidence from komatiites. *Lithos* **30,** 291–307.

PARMAN S. W., DANN J. C., GROVE T. L., and DE WIT M. J. (1997) Emplacement conditions of komatiite magmas from the 3.49 Ga Komati Formation, Barberton Greenstone Belt, South Africa. *Earth Planet. Sci. Lett.* **150,** 303–323.

PEARSON D. G., CARLSON R. W., SHIREY S. B., BOYD F. R., and NIXON P. H. (1995) Stabilisation of Archaean litho-

spheric mantle: A Re-Os isotope study of peridotite xenoliths from the Kaapvaal craton. *Earth Planet. Sci. Lett.* **134,** 341–357.

PYKE D. R., NALDRETT A. J. and ECKSTRAND O. R. (1973) Archean ultramafic flows in Munro Township, Ontario. *Geol. Soc. Amer. Bull.* **84,** 955–978.

SCHMIDT M. W. and POLI S. (1998) Experimentally based water budgets for dehydrating slabs and consequences for arc magma generation. *Earth Planet. Sci. Lett.* **163,** 361–379.

SISSON T. W. and LAYNE G. D. (1993) H_2O in basalt and basaltic andesite glass inclusions from four subduction-related volcanoes. *Earth Planet. Sci. Lett.* **117,** 619–635.

SISSON T. W. and GROVE T. L. (1993) Experimental investigations of the role of H_2O in calc-alkaline differentiation and subduction zone magmatism. *Contrib. Mineral. Petrol.* **113,** 143–166.

SMITH H. S. and ERLANK A. J. (1982) Geochemistry and petrogenesis of komatiites from the Barberton greenstone belt, South Africa. In *Komatiites* (eds. N. T. ARNDT and E. G. NISBET), pp. 347–397, George Allen & Unwin, London.

STONE W. E., JENSEN L. S., and CHURCH W. R. (1987) Petrography and geochemistry of an unusual Fe-rich basaltic komatiite from Boston Township, Ontario. *Canad. J. Earth Sci.* **24,** 2537–2550.

SMITH H. S., ERLANK A. J., and DUNCAN A. R. (1980) Geochemistry of some ultramafic komatiite lava flows from the Barberton Mountain Land, South Africa. *Precambrian Res.* **11,** 399–415.

VILJOEN R. P. and VILJOEN M. J. (1969) Evidence for the existence of a mobile extrusive peridotitic magma from the Komati Formation of the Onverwacht Group. *Geol. Soc. South Africa Spec. Pub. 2, Upper Mantle Project,* 87–112.